Subsynchronous Oscillation Source Location in Power System with High Penetration of Wind Power Using Multivariate Variational Mode Decomposition

This article has been accepted for publication in IEEE Transactions on Power Systems. This is the author's version which has not been fully edited and content may change prior to final publication. Citation information: DOI 10.1109/TPWRS.2025.3560761

Subsynchronous Oscillation Source Location in Power System with High Penetration of Wind Power Using Multivariate Variational Mode Decomposition

Tao Jiang, *Senior Member, IEEE,* Bohan Liu, Xue Li, *Member, IEEE,* Andrea Mazza, *Senior Member, IEEE,* Guoqing Li, Enrico Pons, *Senior Member, IEEE,* Tao Huang, *Senior Member, IEEE*

Abstract—Accurately and promptly extracting subsynchronous oscillation (SSO) components from measurements and locating SSO sources are crucial for SSO suppression. Existing transient energy flow (TEF) based SSO location methods suffer from low location accuracy and poor robustness. To cope with the shortcoming of the traditional TEF in SSO source location, this paper proposes a multivariate variational mode decomposition (MVMD) based SSO source location method to locate the SSO source from the measurements. Firstly, the multi-channel measurement matrix of each generator, including voltage and current measurements, is formed. Then, the multi-channel intrinsic mode functions (IMFs) are simultaneously decomposed from the formed multi-channel measurement matrix by using the MVMD approach, enabling the simultaneous decomposition of SSO components from measurements. Furthermore, the IMFs associated with the SSO mode are identified according to the Hilbert transform (HT). Using the identified IMFs, the MVMD-based TEF is calculated and the SSO source is located. Finally, the performance of the proposed method is evaluated using the simulation data of the modified 4-machine 11-bus test system and the field measurements from the Guyuan SSO event in the North China region. The results validate the accuracy and effectiveness of the proposed method in the SSO source location.

***Index Terms*—power systems, subsynchronous oscillation, oscillation source location, multivariate variational mode decomposition, transient energy flow.**

I. Introduction

Subsynchronous oscillation (SSO) events, caused by large-scale wind power integration, bring new challenges to the security and stability of the power grid [1]-[2]. In recent years, many SSO events caused by grid-connected wind farms have occurred in Texas, USA [3], Minnesota, USA [4], Guyuan, Hebei, China [5] and other places, resulting in a series of accidents (such as large-scale wind turbine off-grid and its crowbar circuit damage, thermal power unit shafting fracture, and conventional unit protection tripping) that seriously restrict the stability of the power system and the reliable consumption of wind power. A large number of SSO events have demonstrated that promptly and accurately locating SSO sources is essential for power grid dispatchers to make reasonable control decisions.

The wide-area measurement system (WAMS), utilizing phasor measurement units (PMU) widely deployed in the power grid, provides rich data support for SSO online monitoring and traceability [6]-[7]. Currently, SSO source location methods based on measurements mainly fall into three categories: AI-based methods [8]-[10], impedance-based methods [11]-[14], and energy-based methods [15]-[19]. The AI-based methods locate the oscillation source by leveraging well-trained SSO source models. For example, a novel deep learning (DL)-based SSO diagnostic method was proposed demonstrating high location accuracy [8]-[9]. In [10], an SSO source location method based on the open-loop modal coupling theory and deep transfer learning (DTL) algorithm was proposed. Although AI-based SSO source location methods have high location accuracy, the physical meaning is not clear, and the location performance depends on the quality of the training dataset. The impedance-power method locates SSO sources by calculating the impedance and the power of SSO modes. In [11], to locate the SSO, the SSO equivalent impedance of each wind farm was calculated in real-time at the SSO frequency. The wind farm with negative SSO equivalent resistance was located as the SSO source. In [12], based on the measured voltage and current, an oscillation source location method considering the frequency coupling effect was proposed to accurately identify the SSO source. Furthermore, in [13], the composition of power system measurements during SSO was analyzed. Prony analysis and the matrix pencil method (MPM) were subsequently employed to extract subsynchronous resonance parameters and calculate SSO impedance/power, facilitating online tracing of SSO. In [14], the SSO wide-area monitoring system framework was further constructed, and the SSO source and oscillation path were identified in real-time by using the aggregated impedance model. Unlike impedance power methods, the energy-based methods construct the energy function and then locate the SSO source according to the energy flow direction of each component in the network. In [15], an SSO traceability method based on subsynchronous modal energy (SSME) was proposed. This method constructs the SSME of each subsystem port and locates the SSO source according to the SSME flow. In [16], the transient energy flow (TEF) method was applied to the forced-type SSO (FSSO) source location. This method uses the fast Fourier transform (FFT) to decompose the voltage and current in the *xy* coordinate system, and then uses the instantaneous value of voltage and current

The authors would like to thank the support in part by NSFC-CSG joint smart grid project (U23B20131); National Natural Science Foundation of China (52377083).

Tao Jiang, Bohan Liu, Xue Li and Guoqing Li are with the Department of Electrical Engineering, Northeast Electric Power University, Jilin, JL 132012 China. (e-mail:tjiang@neepu.edu.cn, 1202100012@neepu.edu.cn, xli@neepu.edu.cn, lgq@neepu.edu.cn)

Andrea Mazza, Enrico Pons and Tao Huang are with the Department of Energy, Politecnico di Torino, Torino, 10129, Italy. (e-mail: andrea.mazza@polito.it, enrico.pons@polito.it, tao.huang@polito.it)

under the SSO frequency to calculate the TEF. The component that continuously injects energy into the network is traced as the SSO source. In [17], the TEF of DFIG was derived and applied to the FSSO source location of DFIG. In [18], the multi-synchro-squeezing transform (MSST) was used to extract the SSO component from the measurements, and then the TEF was calculated by using the time-domain component with SSO mode. In [19], the application of the energy flow method in ISO New England power system was discussed, and the applicability of the energy-based method for locating oscillations dominated by inverter based resources (IBR) was evaluated. Among the above methods, the TEF method has been very mature in the traditional low-frequency oscillation source location application due to its advantages of high location accuracy and clear physical meaning [20]-[23]. Its expansion in the SSO field has also received extensive attention from scholars. However, the key point for using TEF is the accurate extraction of the SSO component from the measurements. The existing research usually uses a single-channel signal processing method to sequentially decompose the measurements of each channel. This approach does not fully consider the data correlation between each measurement channel to extract SSO components simultaneously, potentially reducing the calculation accuracy of TEF and affecting the accuracy of SSO source location.

Aiming at addressing the above aspects, this paper presents an SSO source location method based on multivariate variational mode decomposition (MVMD). Firstly, the multi-channel measurements matrix during the SSO is constructed. Then, MVMD is used to decompose the measurements into a series of IMF components with different oscillation modes. The instantaneous frequency of each IMF component is calculated via Hilbert transform (HT), and the SSO-IMF component in the subsynchronous frequency band is selected according to the set threshold. Furthermore, MVMD-based TEF is proposed to calculate the TEF of each bus using the selected SSO-IMF for locating the SSO source. The main contributions of this paper are threefold:

1) A novel multi-channel parallel processing method is developed for SSO measurements. This distributed method requires the simultaneous decomposition of voltage and current data from PMU substations to determine whether the monitored bus is an SSO source or sink, significantly reducing the computational complexity associated with traditional multi-channel methods that process massive WAMS data.

2) An SSO source online location method using TEF is designed to be suitable for power systems with high penetration of wind. This method establishes a TEF calculation model based on SSO-IMF, ensuring effective TEF computation under a single SSO mode and improving the calculation accuracy of TEF.

3) Scenarios of FSSO and subsynchronous control interaction (SSCI) validate the effectiveness of the proposed method. Comparative analysis with multivariate empirical mode decomposition (MEMD) and VMD demonstrates that the proposed method exhibits higher accuracy and robustness. The feasibility of the proposed method was verified using field measurements in the actual power system.

The rest of this paper is organized as follows. In Section II, the general TEF and MVMD are presented. In Section III, the MVMD-based TEF is developed. Section IV shows the performance of the proposed MVMD-based TEF using simulated measurements from the modified 4-machine 11-bus test system and field PMU measurements from Guyuan in the North China region. Final remarks are drawn in Section V.

II. Brief Description of Theoretical Background

A. Transient Energy Flow (TEF)

TEF method is utilized to identify oscillation sources by tracing energy interactions between dynamic components and the power grid. This approach specifically delineates the TEF originating from bus i through branch L_{ij} into the network, as detailed in [16]:

$$\begin{aligned} W_i &= \int \mathrm{Im}\left(\bar{I}_{ij}^{*}\mathrm{d}\bar{U}_i\right) = \int\left(P_{ij}\mathrm{d}\theta_i + \frac{Q_{ij}}{U_i}\mathrm{d}U_i\right) \\ &= \int[P_{ij}\,2\pi\Delta f_i\mathrm{d}t + Q_{ij}\mathrm{d}(\ln U_i)] \end{aligned} \tag{1}$$

where, Im is the operator obtaining the imaginary part, P_{ij}, $Q_{ij,}$ and I_{ij} are the active power, reactive power, and current on branch L_{ij}, U_i and θ_i are the voltage magnitude and angle at bus i, Δf_i is the frequency variation at bus i, the superscript " * "represents the conjugate operation.

The parameter in (1) is based on phasor, which is unsuitable for direct use in SSO analysis, an alternative computational format reliant on TEF is defined as:

$$W_i = \int (i_{ij,x}\mathrm{d}u_{i,y} - i_{ij,y}\mathrm{d}u_{i,x}) \tag{2}$$

where, i_{ij} represents the instantaneous value of the current on the branch L_{ij}, where, $i_{ij,x,}$ and $i_{ij,y}$ represent its x and y-axis components, respectively. Similarly, u_i represents the instantaneous value of the voltage at bus i; $u_{i,x,}$ and $u_{i,y}$ represent its x and y-axis components, respectively.

The voltage and current within the xy coordinate system, as denoted in (2), can be obtained by transforming the instantaneous values from the abc coordinate system using (3) and (4).

$$\begin{cases} \begin{bmatrix} u_x & u_y \end{bmatrix}^{\mathrm{T}} = \boldsymbol{D}\begin{bmatrix} u_a & u_b & u_c \end{bmatrix}^{\mathrm{T}} \\ \begin{bmatrix} i_x & i_y \end{bmatrix}^{\mathrm{T}} = \boldsymbol{D}\begin{bmatrix} i_a & i_b & i_c \end{bmatrix}^{\mathrm{T}} \end{cases} \tag{3}$$

$$\boldsymbol{D} = \frac{2}{3}\begin{bmatrix} \cos(\omega_0 t+\theta_0) & \cos(\omega_0 t+\theta_0-\frac{2\pi}{3}) & \cos(\omega_0 t+\theta_0+\frac{2\pi}{3}) \\ -\sin(\omega_0 t+\theta_0) & -\sin(\omega_0 t+\theta_0-\frac{2\pi}{3}) & -\sin(\omega_0 t+\theta_0+\frac{2\pi}{3}) \end{bmatrix} \tag{4}$$

where, ω_0 is the synchronous angular frequency and θ_0 is the initial phase angle.

When using TEF to identify SSO sources, it is crucial to simultaneously extract the SSO components of voltage and current measurements in the xy coordinate system using band-pass filtering. The fluctuation pattern observed in TEF reflects transient energy changes in components during SSO. Based on this pattern, SSO sources can be identified: if the transient energy W_i shows a continuous positive trend, it indicates a consistent injection of oscillating energy into the network, categorizing the component as an SSO source. Conversely, if W_i exhibits a continuous negative trend, it indicates the component is consistently absorbing oscillating energy from the network, identifying it as an SSO sink. It is

important to note that in the *abc* coordinate system, the oscillation frequency of voltage and current, f_{abc}, changes when converted to the *xy* coordinate system. This conversion results in instantaneous values of voltage and current with an SSO frequency of $f_{xy} = f_0 - f_{abc}$, where f_0 is the fundamental frequency.

B. Multivariate variational mode decomposition (MVMD)

MVMD is a non-recursive signal decomposition technique that effectively partitions the original signal in the frequency domain and segregates IMF components. It enables this by breaking down the input signal into a sequence of distinct modal signals, each featuring specific sparse properties [24], [25]. In the context of power system *N*-channel measurements $\boldsymbol{X}(t)=[\boldsymbol{x}_1(t), \boldsymbol{x}_2(t),..., \boldsymbol{x}_N(t)]$, the goal of MVMD is to isolate multi-channel IMF components from $\boldsymbol{X}(t)$ as follows:

$$\boldsymbol{X}(t) = \sum_{c=1}^{C} \mathrm{IMF}_c(t) \tag{5}$$

where *C* is the number of IMFs to be decomposed in $\boldsymbol{X}(t)$, and $\mathrm{IMF}_c(t)$ represents the multi-channel IMF component of the *c*-th oscillation mode, i.e., $\mathrm{IMF}_c(t) = [\mathrm{IMF}_{c,1}(t), \mathrm{IMF}_{c,2}(t),..., \mathrm{IMF}_{c,N}(t)]$.

Then the spectrum of each IMF is calculated, and the bandwidth of each IMF is estimated using the Frobenius norm. Consequently, a variational constraint model is constructed to minimize the sum of the bandwidths of each IMF component, as follows:

$$\begin{aligned} &\min_{\{\mathrm{IMF}_{c,n}\},\{\omega_c\}} \sum_c \sum_n \left\| \partial_t \left[\mathrm{IMF}_{c,n}^{+}(t) e^{-j\omega_c t} \right] \right\|_2^2 \\ &s.t. \sum_c \mathrm{IMF}_{c,n}(t) = \boldsymbol{x}_n(t) \quad n = 1,2,...,N \end{aligned} \tag{6}$$

where $\partial_t[\cdot]$ is the partial derivative of time; ω_c is the center frequency of the *c*-th mode extracted by MVMD; $\mathrm{IMF}_{c,n}^{+}(t)$ is the analytic modulation signal of the *c*-th IMF in channel *n*.

For the variational constrained optimization model of multi-channel measurements shown in (6), the corresponding augmented Lagrangian function is constructed as:

$$\begin{aligned} L(\{\mathrm{IMF}_{c,n}\},\{\omega_c\},\lambda_n) = {} & a \sum_c \sum_n \left\| \partial_t \left[\mathrm{IMF}_{c,n}^{+}(t) e^{-j\omega_c t} \right] \right\|_2^2 \\ & + \sum_n \left\| \boldsymbol{x}_n(t) - \sum_c \mathrm{IMF}_{c,n}(t) \right\|_2^2 \\ & + \sum_n \left\langle \lambda_n(t), \boldsymbol{x}_n(t) - \sum_c \mathrm{IMF}_{c,n}(t) \right\rangle \end{aligned} \tag{7}$$

where, $\lambda_n(t)$ is the Lagrange multiplier and *a* is the penalty factor, $\langle \bullet, \bullet \rangle$ is the inner product. Furthermore, the alternate direction method of multipliers (ADMM) is used to solve the variational model, and the estimated *c*-th mode in the *n*-th channel, as well as the center frequency, are updated in the frequency domain.

To summarize, the steps of using MVMD for decomposing multi-channel measurements $\boldsymbol{X}(t)$ are as follows:

1) input the multi-channel measurements $\boldsymbol{X}(t)$, and set: the initialization parameters, the number of modes to be decomposed, *C*, and the penalty factor, *a*;

2) update the mode and central frequency at the *c*-th oscillation frequency in channel *n*;

3) iteratively update the Lagrange multiplier λ_n;

4) repeat the iterative process composed by steps 2) and 3) until the error meets the specified accuracy requirement.

III. Proposed Methodology

The traditional TEF method calculates the TEF to locate the SSO source at the SSO frequency by filtering measurements from each channel individually. This approach fails to maintain consistency in the oscillation modes of each electrical measurement, resulting in low location accuracy. To address this issue, a MVMD-based TEF approach is proposed to locate SSO sources. This method ensures the simultaneous extraction of SSO modes from the measurements, improving accuracy and consistency.

A. Problem formulation of SSO multi-channel measurements

The instantaneous value signal $x(t)$ of voltage or current in the power system during SSO can be expressed as a time-varying exponential function, i.e.:

$$\begin{aligned} x(t) = {} & A_0 \cos(2\pi f_0 t + \varphi_0) \\ & + \sum_{k=1}^{K} A_k e^{\zeta_k t} \cos(2\pi f_k t + \varphi_k) + r(t) \end{aligned} \tag{8}$$

where A_0, f_0, φ_0 are the amplitude, frequency, and initial phase of the fundamental component, respectively. *K* is the number of the SSO mode; A_k, ξ_k, f_k, φ_k are the amplitude, damping factor, frequency, and initial phase of the *k*-th SSO component, respectively; $r(t)$ is the residual and noise.

For the power system's measured voltage and current signals shown in (2), there can be significant differences in the SSO modes included in different measurements. For example, the same SSO mode may appear with a larger amplitude in the current measurements and a lower, less observable amplitude in the voltage measurements, especially in high-noise environments. Due to the limited observability of oscillation modes, the traditional single-channel SSO mode extraction method often results in inconsistent SSO modes being included in the calculation of TEF's electrical parameters. To address this issue, a multi-channel SSO signal analysis model is constructed to simultaneously extract the SSO modes from the measurements by starting from (8) as follows:

$$\begin{cases} \boldsymbol{X} = \begin{bmatrix} \boldsymbol{I}_x & \boldsymbol{I}_y & \boldsymbol{V}_x & \boldsymbol{V}_y \end{bmatrix} \\ \boldsymbol{I}_x = \{I_x(t), t = 1,2,...,l\}, I_x(t) = A_{I,x}\cos(2\pi f_{I,x} t + \varphi_{I,x}) \\ \qquad + \sum_{k=1}^{K} A_{I,x,k} e^{\zeta_{I,x,k} t} \cos(2\pi f_{I,x,k} t + \varphi_{I,x,k}) + r_{I,x}(t) \\ \boldsymbol{I}_y = \{I_y(t), t = 1,2,...,l\}, I_y(t) = A_{I,y}\cos(2\pi f_{I,y} t + \varphi_{I,y}) \\ \qquad + \sum_{k=1}^{K} A_{I,y,k} e^{\zeta_{I,y,k} t} \cos(2\pi f_{I,y,k} t + \varphi_{I,y,k}) + r_{I,y}(t) \\ \boldsymbol{V}_x = \{V_x(t), t = 1,2,...,l\}, V_x(t) = A_{V,x}\cos(2\pi f_{V,x} t + \varphi_{V,x}) \\ \qquad + \sum_{k=1}^{K} A_{V,x,k} e^{\zeta_{V,x,k} t} \cos(2\pi f_{V,x,k} t + \varphi_{V,x,k}) + r_{V,x}(t) \\ \boldsymbol{V}_y = \{V_y(t), t = 1,2,...,l\}, V_y(t) = A_{V,y}\cos(2\pi f_{V,y} t + \varphi_{V,y}) \\ \qquad + \sum_{k=1}^{K} A_{V,y,k} e^{\zeta_{V,y,k} t} \cos(2\pi f_{V,y,k} t + \varphi_{V,y,k}) + r_{V,y}(t) \end{cases} \tag{9}$$

where $\boldsymbol{I}_x$, $\boldsymbol{I}_y$, $\boldsymbol{V}_x$, and $\boldsymbol{V}_y$ are the x-axis component of current on branch L_{ij}, the y-axis component of current on branch L_{ij}, the x-axis component of voltage at bus i and the y-axis component of voltage at bus i, respectively; l is the sample number.

It is important to note that the multi-channel model in the form of (9) can directly utilize local PMU data from the measured bus. This eliminates the need for centralized analysis in a phasor data concentrator (PDC), significantly reducing communication costs.

B. Calculation method of MVMD-based TEF

Firstly, the voltage at bus i and the current on branch L_{ij} are obtained via the PMUs. Subsequently, the instantaneous values of voltage and current, initially in the *abc* coordinate system, are converted into the *xy* coordinate system. Following this transformation, the multi-channel measurements matrix $\boldsymbol{X}_i$, comprising I_x, I_y, V_x and V_y, is formulated:

$$\boldsymbol{X}_i = \begin{bmatrix} \boldsymbol{I}_x \\ \boldsymbol{I}_y \\ \boldsymbol{V}_x \\ \boldsymbol{V}_y \end{bmatrix}^{\mathrm{T}} = \begin{bmatrix} I_x(1) & I_y(1) & V_x(1) & V_y(1) \\ I_x(2) & I_y(2) & V_x(2) & V_y(2) \\ \vdots & \vdots & \vdots & \vdots \\ I_x(l) & I_y(l) & V_x(l) & V_y(l) \end{bmatrix} \tag{10}$$

The MVMD is employed to perform a multi-channel simultaneous decomposition of $\boldsymbol{X}_i$, resulting in a frequency domain mode matrix that delineates distinct oscillation modes. The decomposed Fourier domain mode matrix is:

$$\boldsymbol{T}_i = \begin{bmatrix} \boldsymbol{T}_{I,x}(\omega_1) & \boldsymbol{T}_{I,y}(\omega_1) & \boldsymbol{T}_{V,x}(\omega_1) & \boldsymbol{T}_{V,y}(\omega_1) \\ \boldsymbol{T}_{I,x}(\omega_2) & \boldsymbol{T}_{I,y}(\omega_2) & \boldsymbol{T}_{V,x}(\omega_2) & \boldsymbol{T}_{V,y}(\omega_2) \\ \vdots & \vdots & \vdots & \vdots \\ \boldsymbol{T}_{I,x}(\omega_k) & \boldsymbol{T}_{I,y}(\omega_k) & \boldsymbol{T}_{V,x}(\omega_k) & \boldsymbol{T}_{V,y}(\omega_k) \\ \vdots & \vdots & \vdots & \vdots \\ \boldsymbol{T}_{I,x}(\omega_m) & \boldsymbol{T}_{I,y}(\omega_m) & \boldsymbol{T}_{V,x}(\omega_m) & \boldsymbol{T}_{V,y}(\omega_m) \end{bmatrix} \tag{11}$$

where $\boldsymbol{T}_{I,x}(\omega_k)$, $\boldsymbol{T}_{I,y}(\omega_k)$, $\boldsymbol{T}_{V,x}(\omega_k)$, and $\boldsymbol{T}_{V,y}(\omega_k)$ are the k-th frequency domain mode components of the current x-axis component on branch L_{ij}, current y-axis component on branch L_{ij}, voltage x-axis component at bus i and voltage y-axis component at bus i, respectively.

Then, the inverse Fourier transform is performed on each frequency domain modal component to obtain the corresponding time domain IMF component as:

$$\begin{aligned} \boldsymbol{X}_i &= \sum_{k=1}^{m} \mathbf{IMF}_k \\ &= \sum_{k=1}^{m} \begin{bmatrix} I_{x,k}(1) & I_{y,k}(1) & V_{x,k}(1) & V_{y,k}(1) \\ I_{x,k}(2) & I_{y,k}(2) & V_{x,k}(2) & V_{y,k}(2) \\ \vdots & \vdots & \vdots & \vdots \\ I_{x,k}(l) & I_{y,k}(l) & V_{x,k}(l) & V_{y,k}(l) \end{bmatrix} \end{aligned} \tag{12}$$

where $I_{x,k}(l)$, $I_{y,k}(l)$, $V_{x,k}(l)$ and $V_{y,k}(l)$ are the l-th element of the k-th IMF component of the current x-axis component on branch L_{ij}, current y-axis component on branch L_{ij}, voltage x-axis component at bus i and voltage y-axis component at bus i, respectively.

Since each IMF component decomposed from MVMD represents a single-frequency signal, HT is employed to track the instantaneous oscillation frequency of the IMF [26]. It continuously computes the instantaneous frequency of each IMF component, thereby detecting and isolating the SSO-IMF component. Given that the SSO frequency typically ranges from 5 to 45 Hz, an approach is adopted to identify the SSO-IMF component. This involves computing the average frequency by averaging the instantaneous frequencies of each IMF component within a defined time window using equation (13). Subsequently, the IMF component that exhibits the SSO mode is identified by establishing a frequency detection threshold:

$$f_{\mathrm{low}} \le \mathrm{mean}(f(t)) \le f_{\mathrm{high}} \tag{13}$$

where f_{low} is the lower limit of frequency, taking 5 Hz, f_{high} is the upper limit of frequency, taking 45 Hz, mean(•) denotes the mean average operation to calculate the mean value.

Further, the extracted SSO-IMF can be expressed as:

$$\boldsymbol{X}_{i,\mathrm{SSO}} = \begin{bmatrix} \boldsymbol{I}_{x,\mathrm{SSO}} \\ \boldsymbol{I}_{y,\mathrm{SSO}} \\ \boldsymbol{V}_{x,\mathrm{SSO}} \\ \boldsymbol{V}_{y,\mathrm{SSO}} \end{bmatrix}^{\mathrm{T}} = \begin{bmatrix} I_{x,\mathrm{SSO}}(1) & I_{y,\mathrm{SSO}}(1) & V_{x,\mathrm{SSO}}(1) & V_{y,\mathrm{SSO}}(1) \\ I_{x,\mathrm{SSO}}(2) & I_{y,\mathrm{SSO}}(2) & V_{x,\mathrm{SSO}}(2) & V_{y,\mathrm{SSO}}(2) \\ \vdots & \vdots & \vdots & \vdots \\ I_{x,\mathrm{SSO}}(l) & I_{y,\mathrm{SSO}}(l) & V_{x,\mathrm{SSO}}(l) & V_{y,\mathrm{SSO}}(l) \end{bmatrix} \tag{14}$$

where $\boldsymbol{I}_{x,\mathrm{SSO}}$, $\boldsymbol{I}_{y,\mathrm{SSO}}$, $\boldsymbol{V}_{x,\mathrm{SSO}}$ and $\boldsymbol{V}_{y,\mathrm{SSO}}$ are the SSO-IMF component of current x-axis component on branch L_{ij}, current y-axis component on branch L_{ij}, voltage x-axis component at bus i and voltage y-axis component at bus i, respectively.

For bus i, the SSO-IMF component in (14) can be used to calculate the MVMD-based TEF

$$W_{i,\mathrm{SSO}} = \int (I_{x,\mathrm{SSO}} \mathrm{d}V_{y,\mathrm{SSO}} - I_{y,\mathrm{SSO}} \mathrm{d}V_{x,\mathrm{SSO}}) \tag{15}$$

In (15), the MVMD-based TEF is computed, which simultaneously isolates the SSO component from the multi-channel measurements. This method avoids the interference of extraneous components during TEF computation and significantly improves the accuracy of SSO source location. The proposed criterion for SSO source location can be outlined as follows: if $W_{i,\mathrm{SSO}}$ increases over time, it indicates a consistent injection of oscillation energy into the power grid, identifying it as the SSO source. Conversely, if $W_{i,\mathrm{SSO}}$ decreases over time, it suggests continuous absorption of oscillation energy from the power grid, identifying it as the SSO sink.

C. Scheme of Proposed Methodology

In summary, the flowchart of the proposed SSO source location method based on MVMD is shown in Fig. 1, and the specific steps are as follows:

1) Obtaining the instantaneous values of three-phase voltage and current components and converting them to the *xy* coordinate system.

2) Constructing the multi-channel measurement matrix using (10), and performing simultaneous decomposition using MVMD. Obtaining the IMF components of different oscillation modes as described in (12).

3) Applying HT to each IMF component and selecting the SSO-IMF component using (13).

4) Substituting the selected SSO-IMF into (15) to calculate the MVMD-based TEF of each bus, and locating the SSO source according to the SSO source criterion.

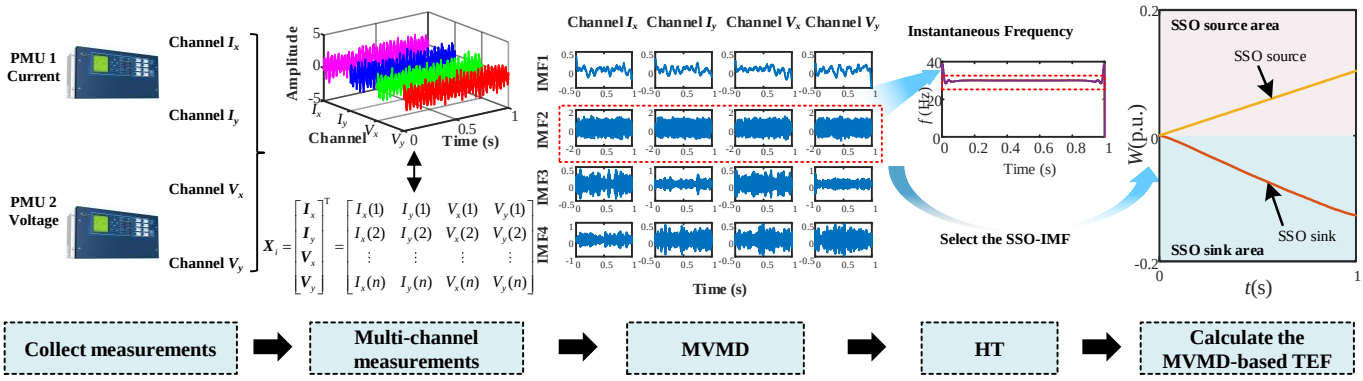

Fig. 1. Flowchart of the proposed MVMD-based SSO source location method

IV. Case Studies

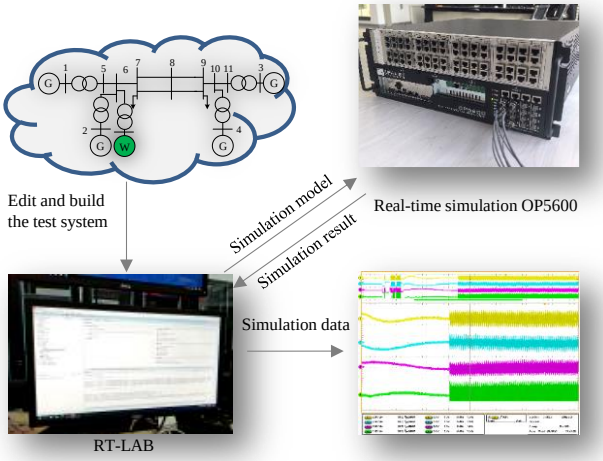

Fig. 2. RT-LAB real-time simulation platform

To verify the accuracy and effectiveness of the proposed MVMD-based SSO source location method, this section conducts analysis and validation using simulation data from the modified 4-machine 11-bus test system and measured SSO data from Guyuan, North China. The simulation platform is depicted in Fig. 2, with a base frequency of 50 Hz.

TABLE I
PARAMETERS OF EACH DFIG IN THE TEST SYSTEM

Name	Value	Name	Value
Capacity	1.5 MW	Rotor reactance	0.16 p.u.
Stator resistance	0.023 p.u.	Excitation reactance	2.9 p.u.
Rotor resistance	0.016 p.u.	Stator reactance	3.08 p.u.

A. Case Description

In this section, simulations are conducted to model forced current source type SSO and SSCI caused by the interaction between wind turbine converters and series compensation in transmission lines. The parameters of DFIG are shown in Table I, and the sampling frequency of the simulation data is 200Hz. The proposed SSO source location method is then analyzed and validated using two scenarios, presented in Section IV.B.

B. Analysis of stationary SSO source location

1) Scenario 1: Forced SSO source

The disturbance is characterized as follows: forced current source with a frequency of 30 Hz and an amplitude of 35 A is applied at the outlet side of the wind farm. This disturbance persists from 3 seconds until the end of the simulation. Fig. 3 illustrates the active power of the wind farm during the occurrence of SSO. According to the FFT analysis of the active power, the corresponding oscillation frequency measures 20.08 Hz.

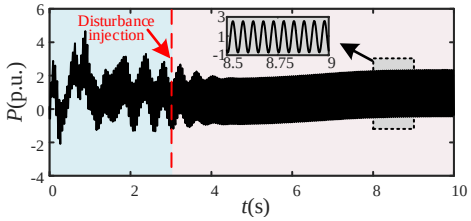

Fig. 3. Active power of wind farm during the SSO in scenario 1

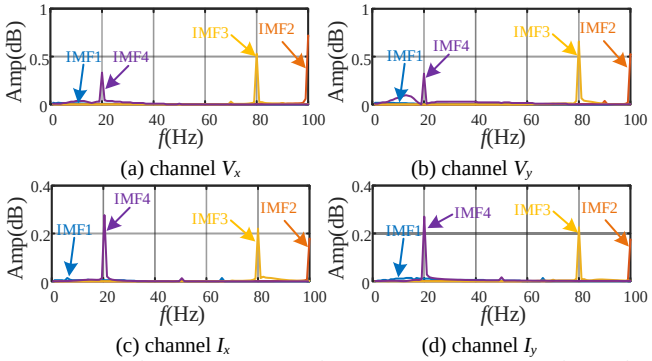

(a) channel V_x (b) channel V_y

(c) channel I_x (d) channel I_y

Fig. 4. Spectra of IMFs decomposed from measurement matrix of wind farm by using MVMD in scenario 1

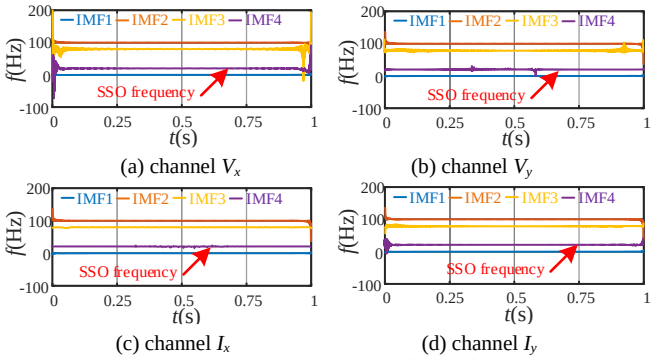

(a) channel V_x (b) channel V_y

(c) channel I_x (d) channel I_y

Fig. 5. HT spectra of the IMFs of each channel of wind farm in scenario 1

Firstly, the instantaneous voltage and current values from the *abc* coordinate system at each bus are transformed to the *xy* coordinate system using (3). Subsequently, (10) is employed to construct the multi-channel measurements matrix comprising I_x, I_y, V_x, and V_y. MVMD is then utilized to decompose the multi-channel measurements matrix, obtaining the IMF components through (12). The spectra of the decomposed IMFs from the wind farm's PCC bus measurements are illustrated in Fig. 4. It can be observed from Fig. 4 that the proposed method effectively achieves simultaneous decomposition of the multi-channel measurements matrix, with each IMF encapsulating distinct oscillation modes.

TABLE II
AVERAGE INSTANTANEOUS FREQUENCY OF EACH IMF

	Channel	IMF1	IMF2	IMF3	IMF4
Average frequency (Hz)	V_x	0.0012	99.98	79.83	**19.98**
	V_y	0.0047	99.89	79.95	**19.96**
	I_x	0.0025	99.94	79.89	**20.01**
	I_y	0.0027	99.92	79.92	**19.93**

Fig. 5 depicts the HT spectrum of the IMF for each measurement channel at the PCC bus of the wind farm. It is evident that the instantaneous oscillation frequency curves of each IMF component exhibit smoothness, resembling single-frequency signals without noticeable modal aliasing, indicating the effective decomposition of the SSO signal by MVMD. Table II provides details of the average instantaneous frequency for each IMF component. IMF4 consistently falls within the subsynchronous frequency band threshold defined by (13), showing an error within 1% compared to the actual SSO frequency. Therefore, IMF4 for each electrical parameter is selected as the SSO component.

Further, the IMF4 component of each electrical parameter is used to compute the MVMD-based TEF via (15), and the result is shown in Fig. 6. It is observed that the MVMD-based TEF of the wind farm exhibits a positive trend, signifying continuous emission of oscillation energy, thus is the SSO source. In contrast, the MVMD-based TEF of the remaining buses demonstrates a negative trend, indicating continuous absorption of oscillation energy and identifying them as the SSO sinks. These identification outcomes are coherent with the simulated disturbance settings, thereby effectively validating the accuracy of the proposed method.

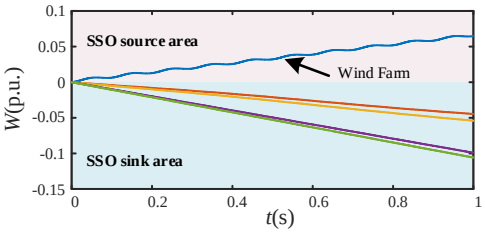

Fig. 6. MVMD-based TEF of buses in scenario 1

Furthermore, the IMF4 component of each electrical parameter is used to compute the MVMD-based TEF via (15), and the result is depicted in Fig. 6. The MVMD-based TEF of the wind farm exhibits a positive trend, indicating continuous emission of oscillation energy and identifying it as the SSO source. In contrast, the MVMD-based TEF of the remaining buses shows a negative trend, signifying continuous absorption of oscillation energy and identifying them as the SSO sinks. These identification outcomes are consistent with the simulated disturbance settings, thereby effectively validating the accuracy of the proposed method.

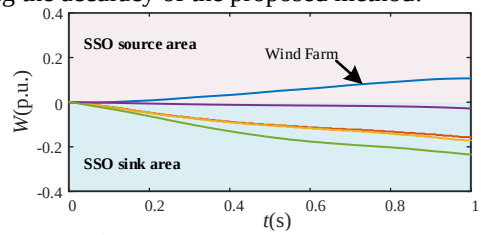

Fig. 7. General TEF of buses in scenario 1

Fig. 7 illustrates the SSO location results using the general TEF approach. It is observed that the results of the general TEF approach are largely consistent with those of the proposed method, thereby effectively validating the accuracy of the proposed method.

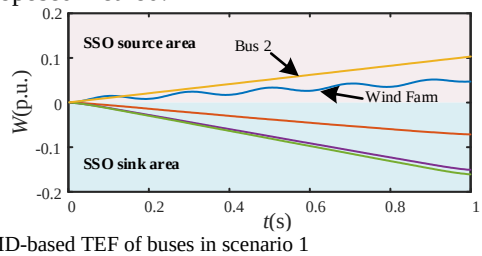

Fig. 8. VMD-based TEF of buses in scenario 1

Fig. 8 further presents the TEF of each bus calculated using variational mode decomposition (VMD) [27]. It can be observed that the VMD-based TEF of the wind farm and bus 2 shows a positive trend, indicating continuous energy injection into the power grid and identifying them as SSO sources. This result contradicts the actual disturbance setting, suggesting misjudgment by the VMD method. By comparing these methods, it is evident that the proposed MVMD-based method can simultaneously and accurately extract the SSO component from the measurements. It effectively avoids the influence of redundant components on TEF calculation and significantly improves the accuracy of SSO source location.

2) Scenario 2: SSCI source

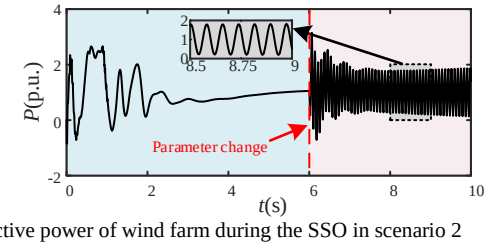

Fig. 9. Active power of wind farm during the SSO in scenario 2

This subsection aims to further validate the accuracy of the proposed method in locating SSCI sources. Using the simulation model introduced in Section IV-A, the line series compensation capacitance parameter is adjusted from 5e-5 to 1e-5 at the 6 second mark within the simulation. Fig. 9 illustrates the active power of the wind farm, showing the occurrence of SSCI. The FFT of the wind farm's active power reveals an oscillation frequency measuring 12.69 Hz.

Employing the proposed approach, MVMD is utilized to

decompose the multi-channel measurements matrix, thereby obtaining the IMF components. The spectra of the decomposed IMFs from the wind farm's PCC bus measurements are depicted in Fig. 10. Subsequently, HT is applied to determine the oscillation frequency of each IMF component, as shown in Fig. 11. Table III provides the average instantaneous frequency of the IMF components across each measurement channel. Remarkably, the IMF4 components within each channel consistently remain within the range defined in (13), with an error within 1% compared to the actual SSO frequency. This result highlights the high accuracy of SSO component extraction achieved by the proposed method. Consequently, by extracting the IMF4 component of each electrical parameter, the MVMD-based TEF is computed and presented in Fig. 12. It can be observed from Fig. 12 that the MVMD-based TEF of the wind farm shows an upward trend, indicating continuous energy injection into the power system and identifying it as the SSO source. Conversely, the MVMD-based TEF of the remaining buses shows a downward trend, indicating continuous absorption of oscillation energy, identifying them as SSO sinks.

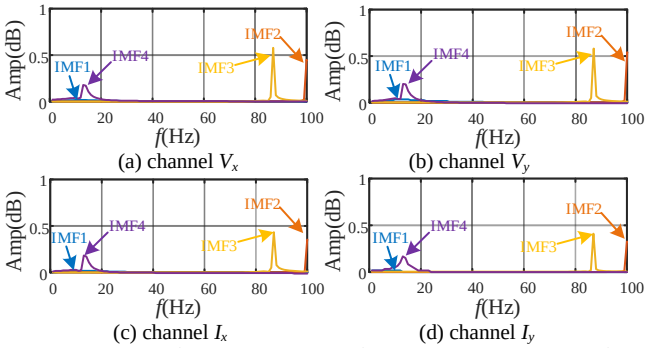

Fig. 10. Spectrums of IMFs decomposed from measurement matrix of wind farm by using MVMD in scenario 2

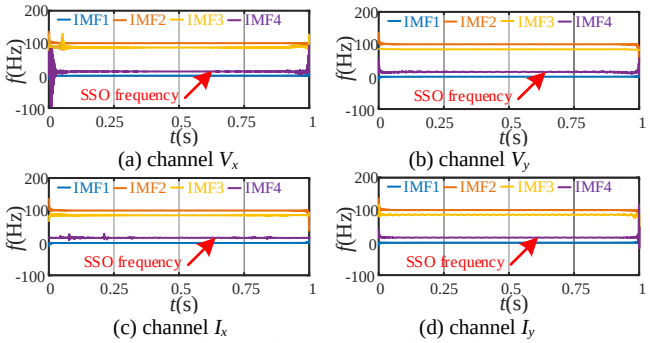

Fig. 11. HT spectrums of IMFs of each channel of wind farm in scenario 2

TABLE III
AVERAGE INSTANTANEOUS FREQUENCY OF EACH IMF

	Channel	IMF1	IMF2	IMF3	IMF4
Average frequency (Hz)	V_x	0.0027	99.98	87.25	**12.78**
	V_y	0.0035	99.98	87.33	**12.75**
	I_x	0.0018	99.97	87.27	**12.81**
	I_y	0.0022	99.98	87.30	**12.77**

Fig. 13 provides a comparative analysis of the SSO components decomposed using the VMD method. This comparison reveals distinct oscillation characteristics encapsulated in the IMF components obtained simultaneously from channel V_x and channel V_y. Specifically, the SSO component extracted from V_x is observed within IMF4, while the SSO component derived from V_y aligns with IMF1. This discrepancy arises from VMD's limitation in comprehensively considering inter-channel data correlation during multi-channel measurement processing, thereby hindering its ability to effectively handle interactions between diverse modes. Consequently, this limitation significantly impacts the efficacy of SSO component decomposition. The failure to achieve simultaneous extraction of SSO components across channels hampers the accuracy of subsequent TEF calculations. Additionally, Fig. 14 presents the VMD-based TEF, which shows a positive trend at bus 4, incorrectly indicating continuous energy injection into the power grid. This inconsistency with the disturbance setting highlights a misjudgment in the SSO source location using VMD.

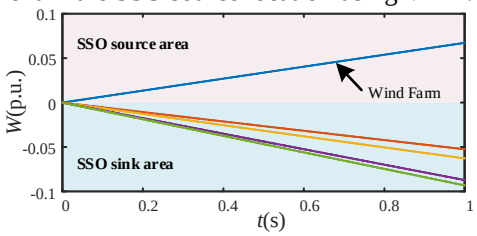

Fig. 12. MVMD-based TEF of buses in scenario 2

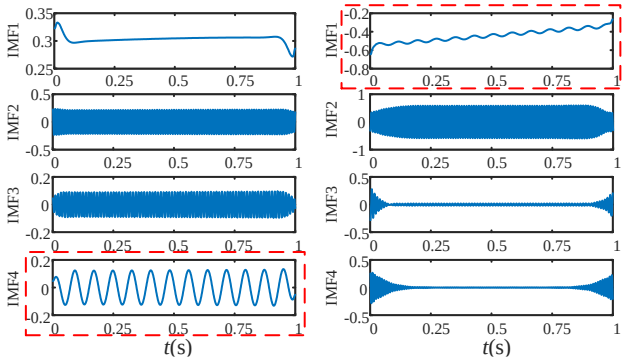

Fig. 13. IMFs decomposed from measurement matrix of wind farm using VMD

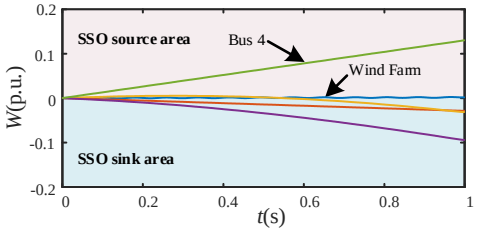

Fig. 14. VMD-based TEF of buses in scenario 2

C. *Analysis of non-stationary SSO source location*

To evaluate the effectiveness of the proposed method in handling non-stationary SSO, a time-varying current source is introduced into the wind farm of the 11-bus test system. Specifically, the oscillation frequency is set to 13 Hz with an amplitude of 0.6 kA during the interval from 0 to 1 second, 15 Hz with an amplitude of 0.7 kA from 1 to 2 seconds, and 18 Hz with an amplitude of 0.8 kA from 2 to 3 seconds. Using the

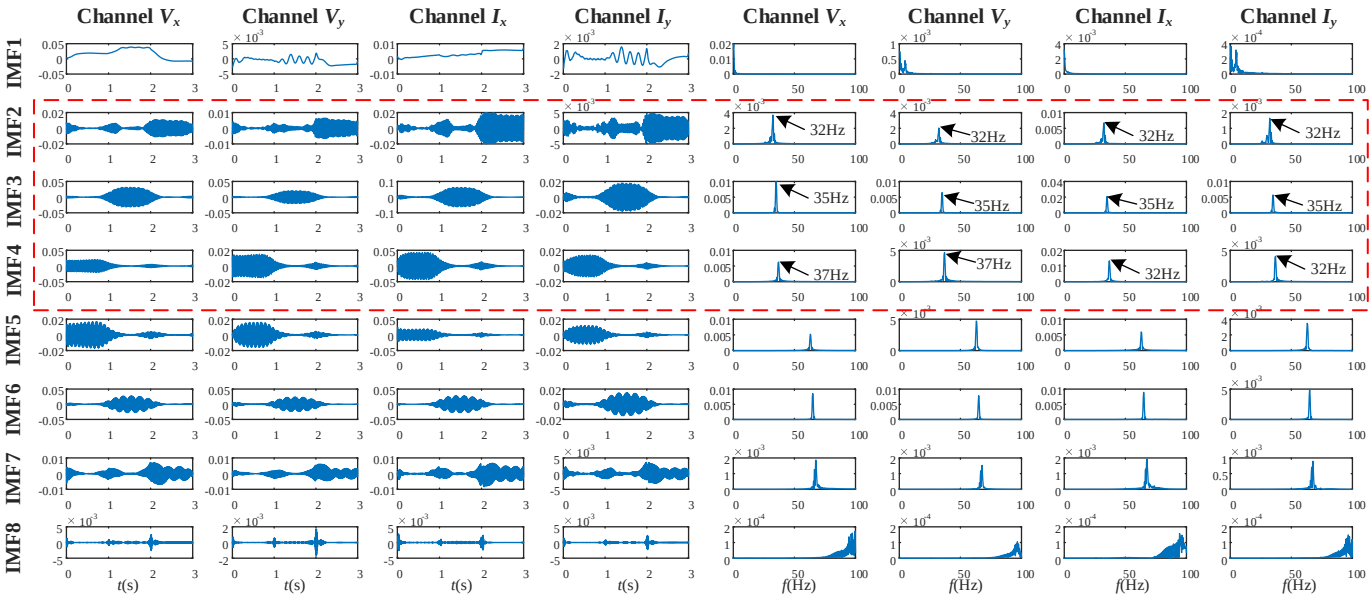

Fig. 15. IMFs and spectrums decomposed from measurement matrix of wind farm by using MVMD in non-stationary SSO scenario

proposed approach, the multi-channel measurement matrix is decomposed into IMF components via MVMD. The decomposed IMFs and the corresponding spectrums of wind farm measurements are depicted in Fig. 15. As shown, the oscillation frequencies of IMF2, IMF3, and IMF4 are 32 Hz, 35 Hz, and 37 Hz, respectively, all within the SSO frequency range. This result aligns with the simulation disturbance settings, confirming that IMF2, IMF3, and IMF4 of each electrical parameter can be selected as the SSO components.

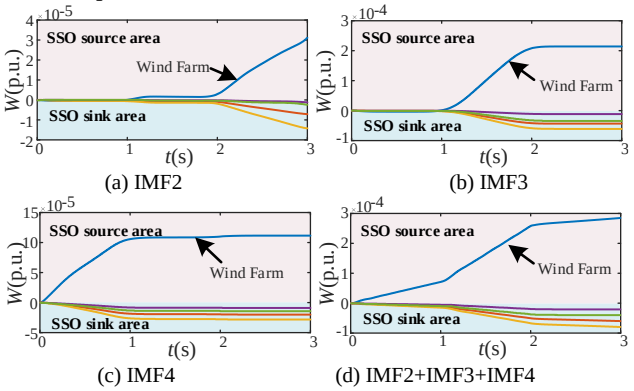

Fig. 16. MVMD-based TEF of buses in non-stationary SSO scenario

Furthermore, the MVMD-based TEF is calculated using IMF2, IMF3, IMF4, and the sum of IMF2, IMF3, IMF4, respectively, with the results presented in Fig. 16. As shown, the TEF curves of wind farm derived from the extracted IMF components all exhibit an upward trend, thereby is the SSO source. This location result aligns with the simulation settings, validating the effectiveness of the proposed method for non-stationary SSO.

It is undeniable that the limitation of the porposed method lies in the difficulty of decomposing the SSO mode into a single IMF. This requires multiple calculations of TEF for different IMFs to locate the SSO source, potentially increasing the computational burden in non-stationary SSO scenario.

D. Robustness analysis

As the measured PMU signals typically include noise components, this section aims to test the robustness of the proposed method in noisy environments. Using the scenario outlined in Section IV-B-1) as an example, Gaussian white noise is injected into the simulation signals to simulate realistic noise conditions. To quantify the effectiveness of SSO-IMF component extraction in a noisy environment, the Shannon entropy index [28] is introduced. Its expression is as follows:

$$H(X) = -\sum_{t=1}^{l} p_t \ln p_t \tag{16}$$

where p_t is the probability distribution at the sample point t. The lower the entropy value and the lower the disorder, the better the IMF signal extraction effect [28].

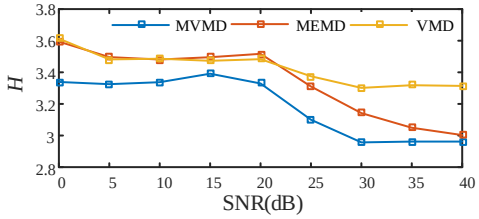

Fig. 17. Comparison of Shannon entropy of SSO-IMFs decomposed by different methods under different Gaussian white noises

Fig. 17 illustrates the entropy of SSO-IMF extracted by MVMD, VMD, and MEMD in various Signal-to-Noise Ratios (SNRs) (i.e., the ratio of signal power to noise power). Compared to MEMD and VMD, the SSO-IMF extracted by MVMD shows a lower Shannon entropy, indicating higher accuracy in extracting SSO components under noises. Fig. 18 presents the decomposition results of these three methods under a 10 dB noise environment. The proposed method successfully isolates the SSO component into IMF4, as demonstrated by its spectrum,

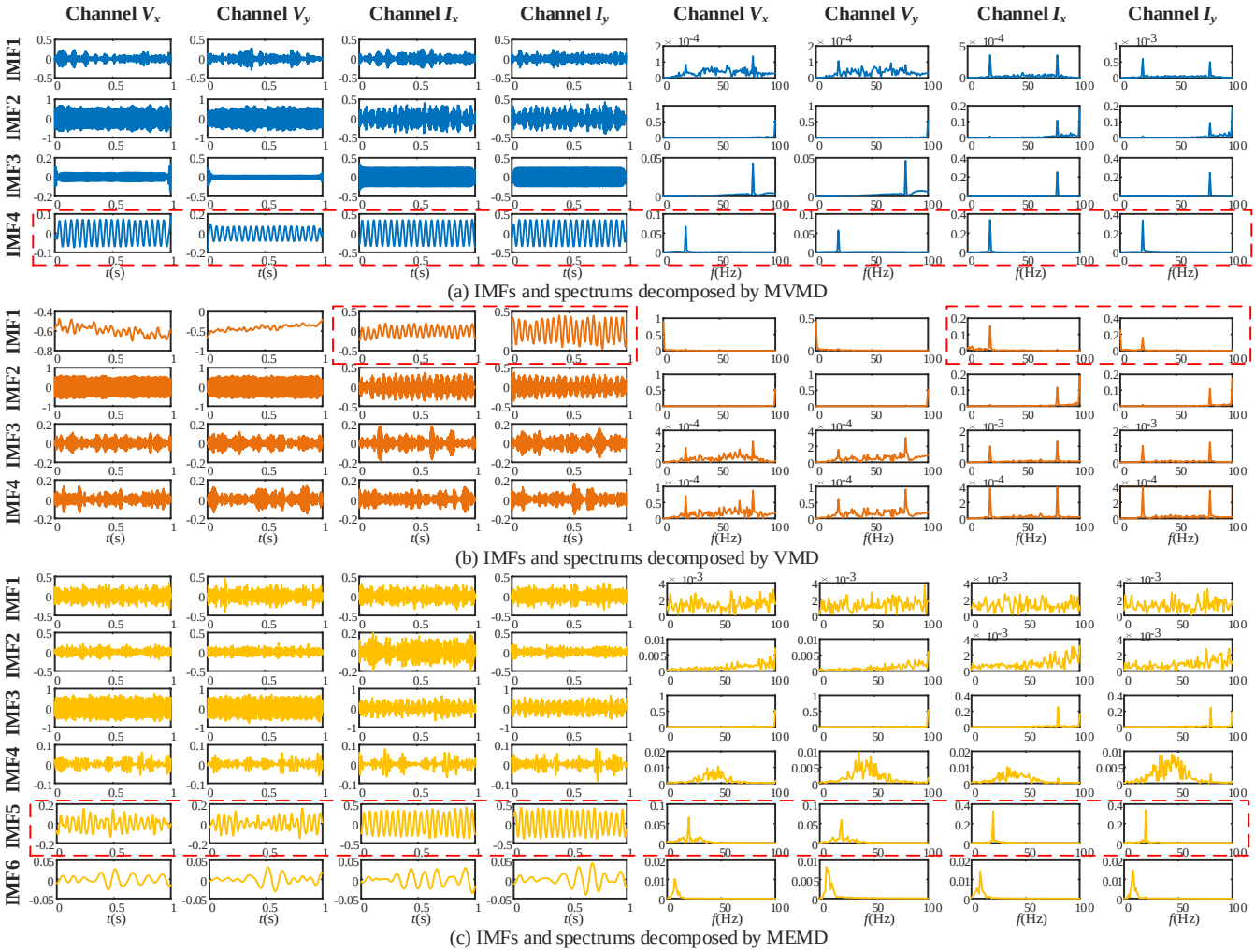

Fig. 18. Comparison of decomposition effects between MVMD, VMD, MEMD under 10dB noise

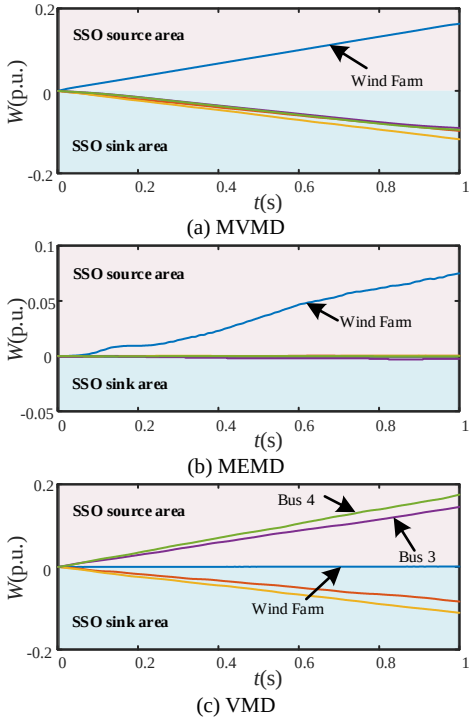

Fig. 19. TEF calculated by different methods under SNR=10dB Gaussian white noise

which shows a prominent peak at 20 Hz. In contrast, the VMD-based method decomposes the current measurements into IMF1, capturing part of the SSO mode, while the voltage measurements suffer from noise interference. The MEMD-based method decomposes the SSO mode into IMF5, which exhibits wide bandwidth and lacks clear frequency constraints, suggesting it includes redundant components. These findings underscore the robustness and effectiveness of the proposed MVMD-based method in accurately extracting SSO components. Fig. 19 shows the TEF calculated by the three methods with SNR=10 dB. The MVMD method effectively identifies the SSO source and SSO sink. The MEMD method only identifies the SSO source and fails to identify the rest of the units as SSO sink. The VMD method fails to simultaneously extract the SSO-IMF components of each channel, resulting in serious misjudgment and failure in the SSO source and SSO sink location. In summary, the proposed method is more robust than other methods and has a great SSO source location performance against the noise.

E. Numerical efficiency analysis

In this subsection, the computational efficiency of the proposed method is analyzed using the example from scenario 1 in Section IV-B-1). The hardware configuration of the

computing platform is CPU Intel Core i7-9750H with a main frequency of 2.6 GHz and 16 GB memory. One second of simulation data was extracted for analysis, with a sampling frequency of 200 Hz, resulting in 200 PMU measurements per channel. The proposed method was compared with VMD and the traditional TEF method, with the results shown in Tab. IV.

TABLE IV
COMPARISON OF NUMERICAL EFFICIENCY

Method	MVMD	VMD	TEF
Time (s)	0.6288	2.2627	0.5589

As shown in Table IV, the proposed method does not significantly increase computation time compared to the traditional TEF method, while offering a notable improvement in computational efficiency over the single-channel VMD method. It should be noted that the computation times represent the total time required for SSO source location, rather than the time specifically for decomposing measurements using the MVMD and VMD algorithms. The proposed multi-channel method allows for the simultaneous selection of SSO-IMFs across multi-channels, whereas VMD requires sequential selection of SSO-IMFs for each channel. This sequential process inevitably increases the overall time when using VMD. Therefore, the proposed method has high computational efficiency and can meet the requirements for online analysis.

F. Measured PMU data of SSO in Guyuan

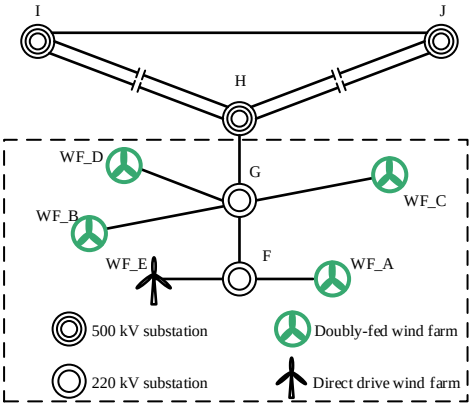

Fig. 20. Partial network topology of the power grid in Guyuan

This section aims to further validate the applicability of the proposed method in actual power systems using the measured data from the Guyuan SSO event in North China. The SSO event occurred on March 2, 2013, characterized by an oscillation frequency of approximately 7 Hz. The installed wind power capacity in this region amounts to roughly 3000 MW. All wind farms, namely WF_A, WF_B, WF_C, WF_D and WF_E, link to the 220 kV substation F and G, thereafter transmitting through two 500 kV lines to the substation I and substation J. The predominant wind turbines in this area are 1.5 MW doubly-fed models, with some utilizing direct-drive technology. The sample frequency is 50 Hz (i.e., 50 points per second are measured). The network topology is shown in Fig. 20.

The multi-channel measurements matrix is constructed for the voltage and current collected by the PMU of each wind farm by using the proposed method. The MVMD is used to obtain the IMF components representing different oscillation modes. Taking the WF_D as an example, the HT spectrum of each IMF component is shown in Fig. 21. The IMF4 oscillation frequency of each electrical quantity is within the detection threshold. The corresponding average oscillation frequencies are 43.15 Hz, 43.21 Hz, 43.17 Hz, and 43.18 Hz, respectively, indicating that the proposed method effectively identifies the SSO frequency. The analysis results of other wind farms are similar to those of plant D. Therefore, IMF4 of each electrical quantity is substituted into (15) as an SSO-IMF component to calculate the MVMD-based TEF of each wind farm and the results are shown in Fig. 22.

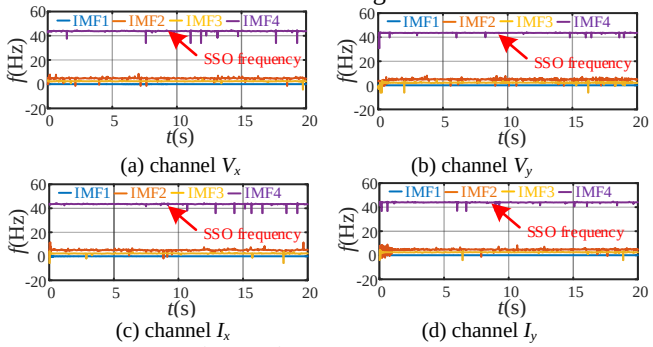

Fig. 21. HT spectrums of IMFs of each channel in WF_D

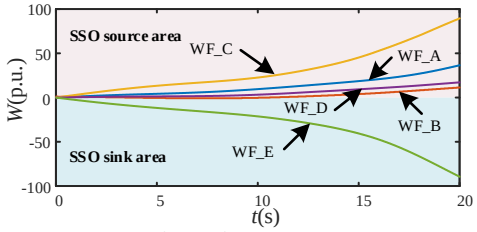

Fig. 22. MVMD-based TEF of wind farms

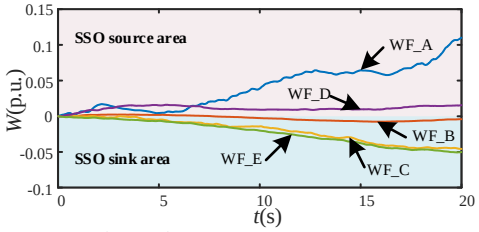

Fig. 23. General TEF of wind farms

It can be observed from Fig. 22 that all plants A, B, C, and D inject energy into the power grid and are the SSO sources, whereas plant E continuously absorbs energy from the power grid and serves as the SSO sink. The above identification results are consistent with the post-event analysis results of this event, which verifies the effectiveness of the proposed method for the actual power grid. Fig. 23 further shows the location result of the general TEF method. The general TEF method is used to misjudge plants B and C as SSO sinks. The reason is that the accuracy of SSO components extracted by bandpass filtering is relatively low, which leads to poor calculation accuracy of TEF and failure in the SSO source location.

In summary, the proposed method calculates the TEF by simultaneously extracting the SSO component in the multi-channel measurements and has higher SSO source location accuracy than the general TEF method.

V. Conclusion

In this paper, a SSO source location method for wind power grid-connected system based on multivariate variational mode decomposition is proposed. The proposed method is analyzed and verified by modified 4-machine 11-bus test system simulation data and Guyuan grid SSO measured data. The conclusions are drawn as follows:

1) compared with the general TEF method, the proposed SSO source location method calculates the TEF by simultaneously extracting the SSO-IMF component in the multi-channel measurements, which has higher SSO source location accuracy;

2) compared with the single channel method, the proposed method decomposes the collected PMU data simultaneously, which effectively avoids the problem that the SSO component between each channel is not synchronized due to the observability of the SSO mode, which affects the location accuracy of the SSO source;

3) robustness analysis indicates that the proposed method effectively extracts SSO components from measurements even under noisy conditions, demonstrating reliable performance in adverse environments;

4) the feasibility of the proposed multi-channel method is further validated using measured PMU data, suggesting its potential for practical application in data-driven SSO source online location systems.

This study enhances the accuracy of traditional TEF methods by synchronously decomposing SSO measurements and extracting SSO modes. The results of the case studies show that the proposed method has good location performance for both stationary SSO and non-stationary SSO. It is foreseeable that although our method has demonstrated effective preprocessing for SSO source location in combination with TEF, it can theoretically be further enhanced by integrating with advanced TEF-based techniques such as complex dissipating energy flow (CDEF). Future work will focus on enhancing the applicability of the TEF method in scenarios, where traditional methods may fail to accurately locate SSO sources.

References

[1] J. Ma and Y. Shen, "Stability assessment of DFIG subsynchronous oscillation based on energy dissipation intensity analysis," IEEE *Trans. Power Electron.*, vol. 35, no. 8, pp. 8074-8087, Aug. 2020.

[2] R. N. Damas, Y. Son, M. Yoon, S. -Y. Kim and S. Choi, "Subsynchronous oscillation and advanced analysis: a review," IEEE *Access*, vol. 8, pp. 224020-224032, 2020.

[3] A. E. Leon and J. A. Solsona, "Sub-Synchronous interaction damping control for DFIG wind turbines," IEEE *Trans. Power Syst.*, vol. 30, no. 1, pp. 419-428, Jan. 2015.

[4] K. Narendra et al., "New microprocessor based relay to monitor and protect power systems against sub-harmonics," 2011 IEEE Electrical Power and Energy Conference, Winnipeg, MB, Canada, 2011, pp. 438-443.

[5] L. Wang, X. Xie, Q. Jiang, H. Liu, Y. Li and H. Liu, "Investigation of SSR in practical DFIG-based wind farms connected to a series-compensated power system," IEEE *Trans. Power Syst.*, vol. 30, no. 5, pp. 2772-2779, Sept. 2015.

[6] Y. Ma, Q. Huang, Z. Zhang and D. Cai, "Application of multisynchrosqueezing transform for subsynchronous oscillation detection using PMU data," IEEE *Trans. Ind. Appl.*, vol. 57, no. 3, pp. 2006-2013, May-June 2021.

[7] H. Liu, Y. Qi, J. Zhao and T. Bi, "Data-driven subsynchronous oscillation identification using field synchrophasor measurements," IEEE *Trans. Power Del.*, vol. 37, no. 1, pp. 165-175, Feb. 2022.

[8] X. Dong, W. Du and H. F. Wang, "Measurement-driven diagnostics of mechanism and source of subsynchronous oscillations in power systems with renewable power generation," IEEE *Trans. Power Syst.*, vol. 39, no. 3, pp. 5366-5381, May 2024.

[9] W. Du, J. Chen, Y. Wang and H. F. Wang, "Measurement-driven source tracing of torsional subsynchronous oscillations caused by open-loop modal resonance," IEEE *Trans. Instrum. Meas.*, vol. 71, pp. 1-14, 2022, Art no. 2502114.

[10] B. Ren, Q. Li, C. Wang, Q. Zhou and R. Sun, "A tracing approach for a subsynchronous oscillation source in a power system with grid-connected PMSG," 2021 IEEE Sustainable Power and Energy Conference (iSPEC), Nanjing, China, 2021, pp. 197-202.

[11] X. Xie, W. Liu, H. Liu, Y. Du and Y. Li, "A system-wide protection against unstable SSCI in series-compensated wind power systems," IEEE *Trans. Power Del.*, vol. 33, no. 6, pp. 3095-3104, Dec. 2018.

[12] X. Xie, Y. Zhan, J. Shair, Z. Ka and X. Chang, "Identifying the source of subsynchronous control interaction via wide-area monitoring of sub/super-synchronous power flows," IEEE *Trans. Power Del.*, vol. 35, no. 5, pp. 2177-2185, Oct. 2020.

[13] Y. Wang, X. Jiang, X. Xie, X. Yang and X. Xiao, "Identifying sources of subsynchronous resonance using wide-area phasor measurements," IEEE *Trans. Power Del.*, vol. 36, no. 5, pp. 3242-3254, Oct. 2021.

[14] N. Ma, X. Xie, P. Kang, et al, " Wide-area monitoring and analysis of subsynchronous oscillation in power systems with high-penetration of wind power," Proceedings of the CSEE, vol. 41, no. 1, pp. 65-74+398, Jan. 2021.

[15] X. Chen, X. Wu, H. Yang, C. Wu and B. Wang, "Sub-synchronous modal energy-based method for locating SSO sources in power systems with DFIGs," IEEE *Trans. Power Del.*, vol. 38, no. 5, pp. 3712-3728, Oct. 2023.

[16] Y. Ren, X. Wang, L. Chen, et al, " Component damping evaluation in sub-synchronous oscillation based on transient energy flow method," IET *Gener. Transm. Distrib.*, vol. 14, no. 3, pp. 460-469, 2020.

[17] N. Cao, X. Zhao, Q. Yu, " Forced oscillation source location of doubly-fed wind turbine based on transient energy flow," Automation of Electric Power Systems, vol. 44, no. 10, pp. 103-110, 2020.

[18] Y. Ma, Q. Huang, H. B. Gooi, Z. Zhang, X. Yang and Y. Wang, "Subsynchronous oscillation analysis using multisynchrosqueezing transform and dissipating energy flow method," IEEE *Trans. Ind. Appl.*, vol. 58, no. 3, pp. 3134-3141, May-June 2022.

[19] S. Maslennikov, "Enhancing the efficiency of locating the oscillation source," IEEE *Trans. Power Syst.*, vol. 39, no. 6, pp. 7257-7265, Nov. 2024.

[20] S. Maslennikov and E. Litvinov, "ISO New England experience in locating the source of oscillations online," IEEE *Trans. Power Syst.*, vol. 36, no. 1, pp. 495-503, Jan. 2021.

[21] Maslennikov S, B. Wang and Litvinov E, " Dissipating energy flow method for locating the source of sustained oscillations," *Int. J. Electr. Power Energy Syst.*, vol. 88, pp. 55-62, 2017.

[22] M. Ghorbaniparvar, "Survey on forced oscillations in power system," *J. Modern Power Syst. Clean Energy*, vol. 5, no. 5, pp. 671-682, September 2017.

[23] P. Gill Estevez, P. Marchi, C. G. Galarza, et al, "Forced oscillation identification and filtering from multi-channel time-frequency representation," IEEE *Trans. Power Syst.*, vol. 38, no. 2, pp. 1257–1269, March 2023.

[24] N. u. Rehman and H. Aftab, "Multivariate variational mode decomposition," IEEE *Trans. Signal Process.*, vol. 67, no. 23, pp. 6039-6052, Dec. 2019.

[25] Q. Song, X. Jiang, S. Wang, J. Guo, W. Huang and Z. Zhu, "Self-Adaptive multivariate variational mode decomposition and its application for bearing fault diagnosis," IEEE *Trans. Instrum. Meas.*, vol. 71, pp. 1-13, 2022, Art no. 3503913.

[26] D. S. Laila, A. R. Messina and B. C. Pal, "A refined Hilbert–Huang transform with applications to interarea oscillation monitoring," IEEE *Trans. Power Syst.*, vol. 24, no. 2, pp. 610-620, May 2009.

[27] K. Dragomiretskiy and D. Zosso, "Variational mode decomposition," IEEE *Trans. Signal Process.*, vol. 62, no. 3, pp. 531-544, Feb. 2014.

[28] M. M. Christiansen and K. R. Duffy, "Guesswork, Large Deviations, and Shannon Entropy," IEEE *Trans. Inf. Theory.*, vol. 59, no. 2, pp. 796-802, Feb. 2013.